

## High Spectral Resolution Lidar Instrument Handbook

J. Goldsmith

April 2016

## **DISCLAIMER**

This report was prepared as an account of work sponsored by the U.S. Government. Neither the United States nor any agency thereof, nor any of their employees, makes any warranty, express or implied, or assumes any legal liability or responsibility for the accuracy, completeness, or usefulness of any information, apparatus, product, or process disclosed, or represents that its use would not infringe privately owned rights. Reference herein to any specific commercial product, process, or service by trade name, trademark, manufacturer, or otherwise, does not necessarily constitute or imply its endorsement, recommendation, or favoring by the U.S. Government or any agency thereof. The views and opinions of authors expressed herein do not necessarily state or reflect those of the U.S. Government or any agency thereof.

# **High Spectral Resolution Lidar Instrument Handbook**

J Goldsmith, Sandia National Laboratories

April 2016

Work supported by the U.S. Department of Energy,  
Office of Science, Office of Biological and Environmental Research

## Acronyms and Abbreviations

ACAPEX	ARM Cloud Aerosol Precipitation Experiment
AMF2	second ARM Mobile Facility
AMIE	ARM Madden Julian Oscillation Investigation Experiment
ARM	Atmospheric Radiation Measurement Climate Research Facility
BAECC	Biogenic Aerosols—Effects on Clouds and Climate
cm	centimeter
DOE	U.S. Department of Energy
FOV	field of view
GHz	gigahertz
HSRL	High Spectral Resolution Lidar
kHz	kilohertz
km	kilometer
m	meter
MAGIC	Marine ARM GPIC Investigation of Clouds
mm	millimeter
mW	milliwatt
nm	nanometer
ns	nanosecond
NSA	North Slope of Alaska
STORMVEX	Storm Peak Lab Cloud Property Validation Experiment

## Contents

Acronyms and Abbreviations .....	iii
1.0 General Overview .....	1
2.0 Mentor Contact Information .....	1
3.0 Vendor/Developer Contact Information .....	1
4.0 Instrument Description .....	1
5.0 Measurements Taken .....	2
6.0 Technical Specifications .....	4
7.0 Instrument System Functional Diagram .....	5
8.0 Instrument/Measurement Theory .....	5
9.0 Setup and Operation of Instrument .....	6
10.0 Software .....	7
11.0 Calibration .....	7
12.0 Safety	9
13.0 Citable References .....	9

## Figures

1. Measurements from the HSRL in Barrow, Alaska .....	3
2. Measurements from the AMF2 HSRL in Hyytiälä, Finland .....	4
3. Schematic of the HSRL .....	5
4. qSpectral profile of backscattering from a mixture of molecules and aerosols .....	6
5. HSRL with its protective cover removed (in background) .....	7
6. Calibration scan .....	9

## Tables

1. HSRL campaign participation as part of AMF2 .....	2
--	---

## 1.0 General Overview

High Spectral Resolution Lidar (HSRL) systems provide vertical profiles of optical depth, backscatter cross-section, depolarization, and backscatter phase function. All HSRL measurements are absolutely calibrated by reference to molecular scattering, which is measured at each point in the lidar profile. Like the Raman lidar but unlike simple backscatter lidars such as the micropulse lidar, the HSRL can measure backscatter cross-sections and optical depths without prior assumptions about the scattering properties of the atmosphere. The depolarization observations also allow robust discrimination between ice and water clouds. In addition, rigorous error estimates can be computed for all measurements. A very narrow, angular field of view reduces multiple scattering contributions. The small field of view, coupled with a narrow optical bandwidth, nearly eliminates noise due to scattered sunlight. There are two operational U.S. Department of Energy (DOE) Atmospheric Radiation Measurement (ARM) Climate Research Facility HSRL systems, one at the Barrow North Slope of Alaska (NSA) site and the other in the second ARM Mobile Facility (AMF2) collection of instrumentation.

## 2.0 Mentor Contact Information

John Goldsmith  
Sandia National Laboratories  
P.O. Box 969, MS9406  
Livermore, CA 94551-0969  
Phone: 925-294-2432  
E-mail: [jgold@sandia.gov](mailto:jgold@sandia.gov)

## 3.0 Vendor/Developer Contact Information

Edwin Eloranta  
University of Wisconsin  
1225 W. Dayton Street  
Madison, WI 53706  
Phone: 608-262-7327  
E-mail: [eloranta@ssec.wisc.edu](mailto:eloranta@ssec.wisc.edu)

## 4.0 Instrument Description

The key design features of the ARM HSRL systems are summarized here. They are designed for long-term unattended operation, controlled remotely, and operated as Internet appliances. Additional details are provided later.

The laser transmitter is a diode-pumped, intracavity frequency-doubled Nd:YAG laser. Narrow-band, single-frequency operation is provided by injection seeding with a single-frequency, cw-diode-pumped diode laser. The main laser cavity is maintained in resonance with the seed laser by adjusting the cavity

length to minimize the time between the Q-switch trigger and the emission of the laser pulse. The emission wavelength is tuned via temperature control of the seed laser crystal and is locked to line #1109 of the iodine absorption spectra. Locking is accomplished by minimizing the transmission through a 2-cm-long iodine absorption cell. The use of a high-repetition-rate laser and expansion of the transmitted beam through a 400-mm telescope reduces the transmitted energy density to eye-safe levels; thus, it is possible to look directly into the output beam without hazard.

The receiver and transmitter use the same afocal telescope, simplifying the maintenance of stable alignment of the transmitter and receiver, although the angular field-of-view (FOV) is only 45  $\mu$ rad. The small FOV and the 4 kHz repetition rate also limit the near-field signal strength, making it possible to record continuous profiles that start at an altitude of  $\sim$ 50 m and extend to 30 km using photon-counting detectors. The small FOV also suppresses multiple scattering contributions.

## 5.0 Measurements Taken

Two HSRL systems are operated by the ARM Climate Research Facility (for a description of other systems, see <http://lidar.ssec.wisc.edu/>). One system is resident at the NSA site in Barrow, where it has been operational since March 2011. The other system is one of the instruments in AMF2. As part of that facility, the system has participated in the campaigns listed in Table 1. Sample results from the two systems are presented in Figure 1 and Figure 2.

**Table 1.** HSRL campaign participation as part of AMF2.

Start	Finish	Campaign	Location	Website
11/15/2010	4.25/2011	STORMVEX	Steamboat Springs, Colorado	<a href="http://www.arm.gov/sites/amf/sbs/">http://www.arm.gov/sites/amf/sbs/</a>
10/1/2011	3/31/2012	AMIE	Gan Island, Maldives	<a href="http://www.arm.gov/campaigns/twp2011amie-manus">http://www.arm.gov/campaigns/twp2011amie-manus</a>
10/1/2012	9/30/2013	MAGIC	Voyage Los Angeles to Hawaii	<a href="http://www.arm.gov/sites/amf/mag/">http://www.arm.gov/sites/amf/mag/</a>
2/1/2014	9/13/2014	BAECC	Hyytiälä, Finland	<a href="http://www.arm.gov/sites/amf/tmp/">http://www.arm.gov/sites/amf/tmp/</a>
1/12/2015	2/12/2015	CAPEX	Voyage, Hawaii to San Diego	<a href="http://www.arm.gov/camplaigns/amf2015apex">http://www.arm.gov/camplaigns/amf2015apex</a>

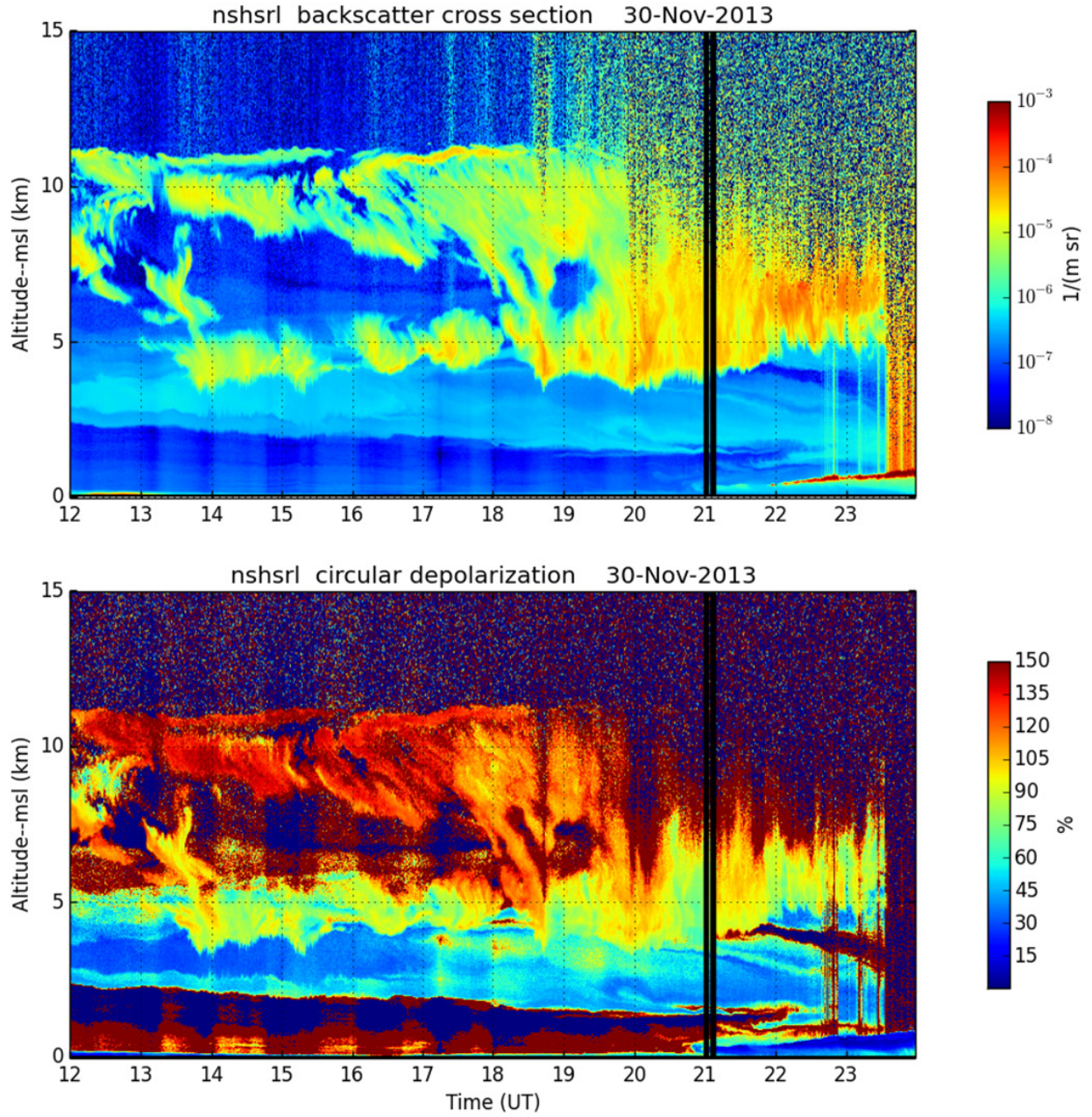


**Figure 1.** Measurements from the HSRL in Barrow, Alaska.

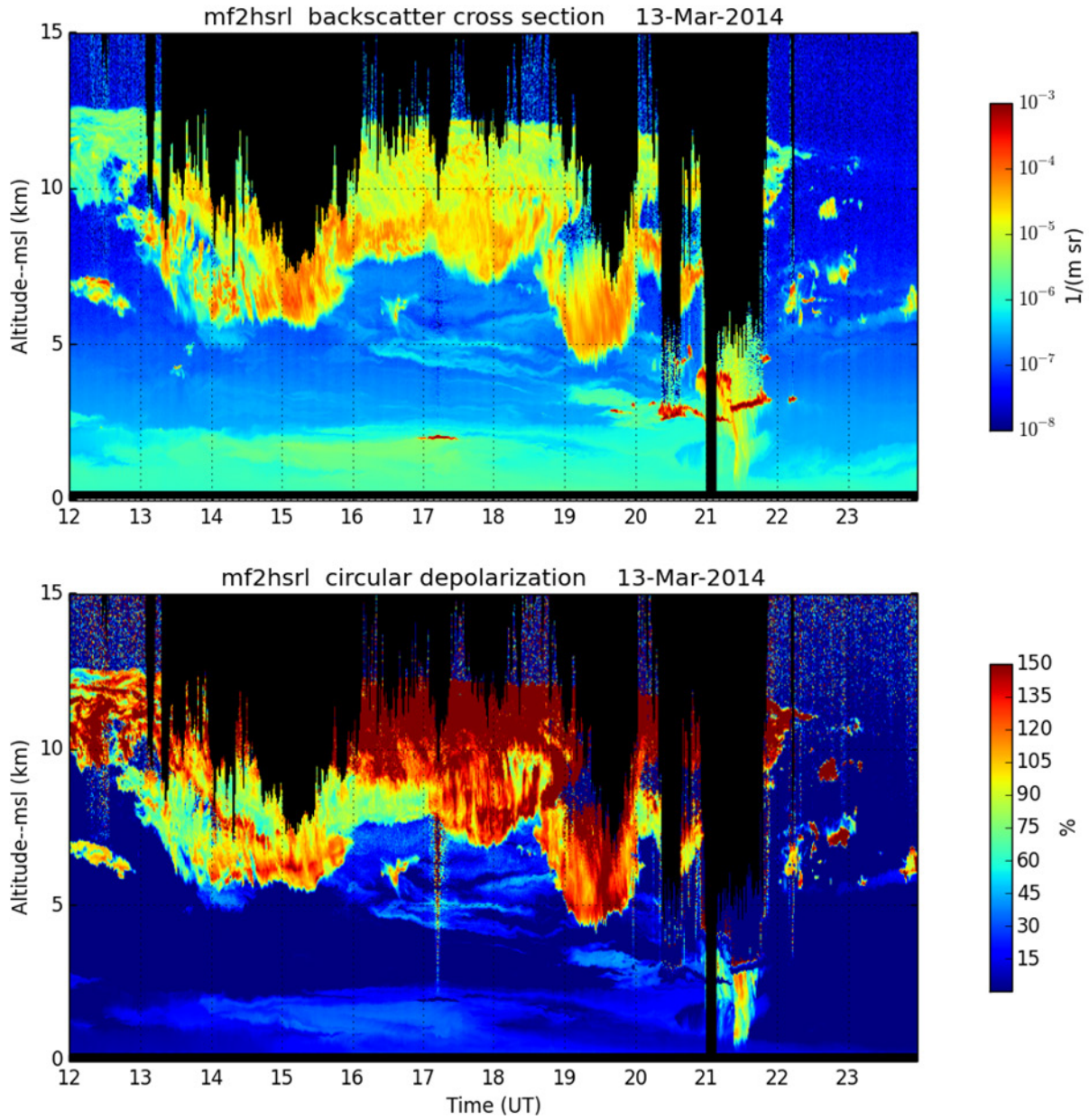


Figure 2. Measurements from the AMF2 HSRL in Hyytiälä, Finland.

## 6.0 Technical Specifications

Transmitted power-----400 mw  
Wavelength-----532 nm (locked to line 1109 of iodine)  
Laser pulse width-----40 ns  
Repetition rate-----4 kHz  
Receiver field-of-view-----45 microradians  
Receiver aperture-----40 cm  
Receiver spectral bandpass-----6 GHz (pressure tuned etalon)

Aerosol blocking filter bandwidth—1.8 GHz (line 1109 of iodine spectrum)  
 Molecular channel detector-----Perkin-Elmer SPCM-ARQ-13, QE ~50% @532 nm  
 High gain combined channel detector—Perkin-Elmer SPCM-ARQ-12  
 Low gain combined channel detector—Perkin-Elmer SPCM-ARQ-12FC  
 Cross Polarization channel detector—Perkin-Elmer SPCM-ARQ-12FC  
 Data acquisition-----Photon counting  
 Altitude resolution-----7.5 m (50 nsec) bin width  
 Altitude range recorded-----0---->30 km  
 Typical time resolution-----.5 s (programmable)

## 7.0 Instrument System Functional Diagram

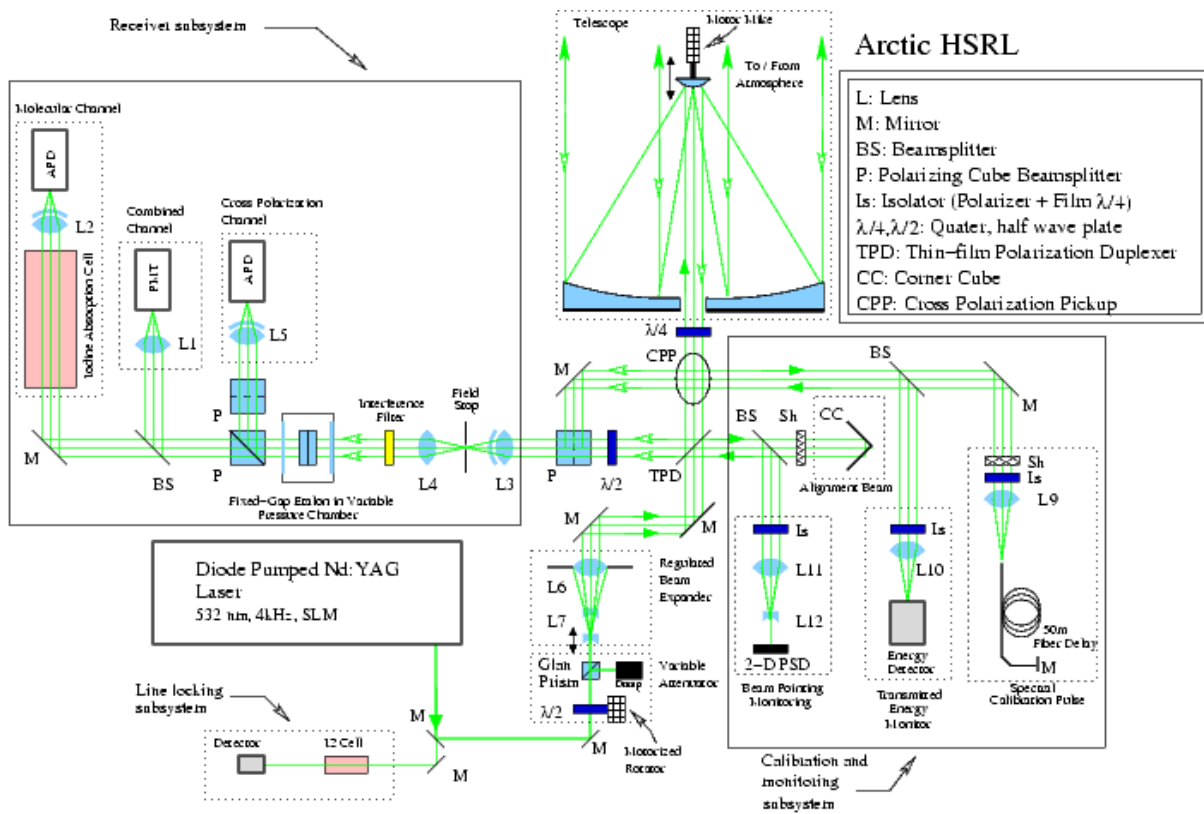
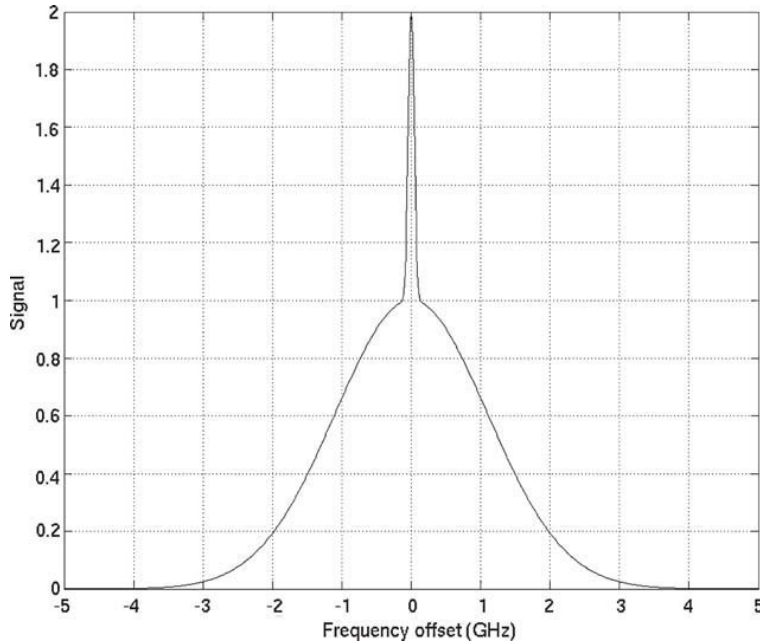


Figure 3. Schematic of the HSRL.

## 8.0 Instrument/Measurement Theory

Two primary optical mechanisms are responsible for the production of a lidar signal: backscatter of the laser beam by particles (including molecules) and attenuation of the laser beam before it reaches the region and of the backscattered light before it is detected. Thus, at least two measurements must be made in order to determine these two atmospheric unknowns (attenuation and backscatter coefficients). A simple backscatter lidar provides only one measurement, making it necessary to assume a functional

dependence of these two unknowns (the Klett method). The HSRL method avoids this assumption by the use of two measured profiles instead of just one. Specifically, this method uses the Doppler frequency shifts produced when photons are scattered from molecules in random thermal motion. The Maxwellian distribution of molecular velocities has a width of  $\sim 300$  m/s that produces Doppler shifts of  $\sim 1$  GHz. In contrast, aerosols, cloud particles, and other particulate matter move with velocities determined by the wind ( $\sim 10$  m/s) and turbulence ( $\sim 1$  m/s) producing Doppler shifts of  $\sim 30$  MHz and  $\sim 3$  MHz, respectively. As a result, the frequency distribution of light backscattered from the atmosphere consists of a narrow spike near the frequency of the laser transmitter caused by particulate scattering riding on a much broader distribution produced by molecular scattering (Figure 4).



**Figure 4.** Spectral profile of backscattering from a mixture of molecules and aerosols.

HSRLs use optical filters to distinguish between photons scattered from molecules and those scattered by aerosol or cloud particles. Very narrow bandwidth filters ( $\sim 1$  GHz) are required. In addition, the transmitting laser frequency must be locked to the filter center frequency, and the linewidth must be smaller than the filter width ( $\sim 100$  MHz). These requirements make HSRLs difficult to implement, but they provide relatively large molecular signals and can use very narrow bandwidths to block solar noise.

## 9.0 Setup and Operation of Instrument

All components of the HSRL are located on a single assembly, as shown in (Figure 5). Once the instrument is in place beneath a suitable window, operation can begin simply after establishing power and Ethernet connections. All start-up and calibration procedures are performed by the onboard computer and can be controlled remotely. The only manual function required by the operator is to cover the output of the telescope during a specified period of the otherwise-automated calibration procedure.



**Figure 5.** HSRL with its protective cover removed (in background).

## 10.0 Software

As mentioned in the preceding section, the system operation is fully automated using software relevant in the HSRL processor. As of the writing of this document, data collection and processing are performed by automated routines run at the University of Wisconsin and are subsequently sent to the ARM Data Archive. Plans are being developed to transfer the data collection and processing routines to the ARM Climate Research Facility.

## 11.0 Calibration

The signals  $S_c$  and  $S_m$  (equations 1a and 1b) detected in the combined channel and in the molecular channel, respectively (**Error! Reference source not found.**), can be described as a linear combination of the number  $N_a$  of aerosol photons and the number  $N_m$  of molecular photons incident on the lidar receiver:

$$S_c = N_a + C_{mc} N_m$$

$$S_m = C_{am} N_a + C_{mm} N_m \quad (1a \text{ and } 1b)$$

The equations have been normalized relative to the response of the combined channel to aerosol photons. This normalization is possible because an absolute calibration is generated by comparing the observed molecular lidar return to the lidar return computed from Rayleigh scattering theory.  $C_{mc}$  describes the relative contribution of molecular photons to the combined channel.  $C_{mc}$  may be less than unity if the pre-filter used to block sunlight is sufficiently narrow to affect the transmission of the Doppler-broadened molecular scattering.  $C_{am}$  describes the response of the molecular channel to aerosol photons and accounts for the online leakage of the absorption filter.  $C_{mm}$  describes the transmission of molecular photons through the absorption filter. Equations 1a and 1b can be inverted (equations 2a and 2b) to compute the relative number of aerosol and molecular photons incident on the system:

$$N_a = \frac{C_{mm} S_c - C_{mc} S_m}{C_m - C_{am} C_{mc}}$$

$$N_m = \frac{S_m - C_{am} S_c}{C_{mm} - C_{am} C_{mc}} \quad (2a \text{ and } 2b)$$

The coefficients  $C_{am}$ ,  $C_{mm}$ , and  $C_{mc}$  are determined by directing a sample of the transmitted beam into the receiver while scanning the laser frequency. The spectral transmissions (Figure 6) for the molecular and combined channel are then convolved with the Doppler-broadened molecular spectrum, which is computed from theory and independently supplied temperature data.  $C_{mm}$  and  $C_{mc}$  are the values of the molecular and combined convolution functions at the operating frequency of the laser. Because  $C_{mm}$  and  $C_{mc}$  are temperature and pressure dependent, they must be computed as functions of altitude.  $C_{am}$  is taken directly from the measured leakage of the absorption filter at the operating frequency of the laser. Figure 6 displays a calibration scan showing the transmission of the molecular (blue) and combined (green) channels as a function of frequency. The Doppler-broadened molecular spectrum for 300 K is also shown (black). Line 1109 of the iodine absorption spectrum (central notch) rejects most of the aerosol scattering and the central portion of the molecular scattering while passing the wings of the molecular line. The spectral transmission of the combined channel is determined by the pre-filter etalon.

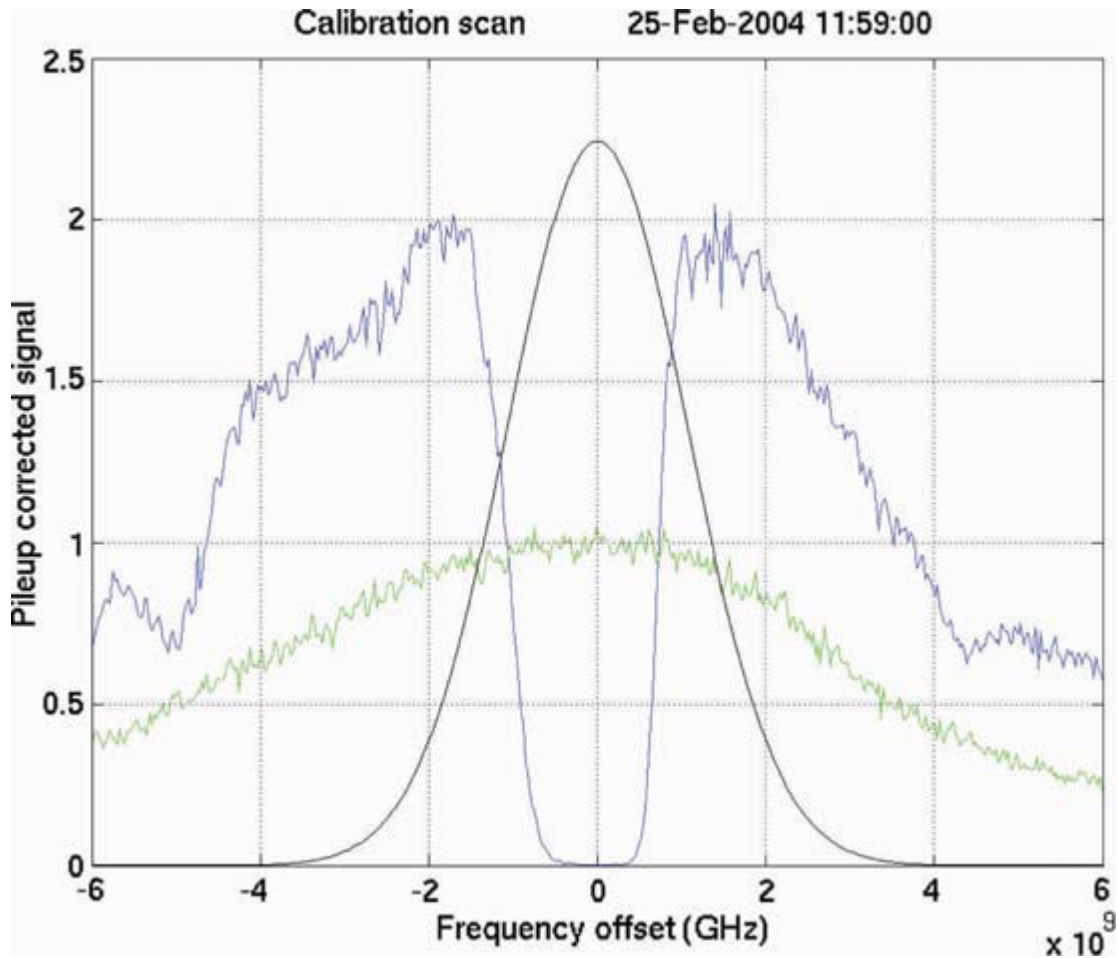


**Figure 6.** Calibration scan.

## 12.0 Safety

The system is completely enclosed during normal operation (the cover is shown to the rear of Figure 5), which protects personnel from any hazardous laser beams or voltages. The output laser beam is transmitted through the top of the assembly, but use of a high-repetition-rate laser and expansion of the transmitted beam through a 400-mm telescope reduce the transmitted energy density to eye-safe levels. It is possible to look directly into the output beam without hazard.

## 13.0 Citable References

Ackerman, SA, RE Holz, R Frey, EW Eloranta, B Maddux, and M McGill. 2008. "Cloud detection with MODIS: Part II Validation." *Journal of Atmospheric and Oceanic Technology* 25: 1073-1086, [doi:10.1175/2007JTECHA1053.1](https://doi.org/10.1175/2007JTECHA1053.1).

- Bourdages, L, TJ Duck, G Lesins, JR Drummond, and EW Eloranta. 2009. "Physical properties of High Arctic tropospheric particles during winter." *Atmospheric Chemistry and Physics* 9: 6881-6897, [doi:10.5194/acp-9-6881-2009](https://doi.org/10.5194/acp-9-6881-2009).
- de Boer, G, EW Eloranta, and MD Shupe. 2009. "Arctic mixed-phase stratiform cloud properties from multiple years of surface-based measurements at two high-latitude locations." *Journal of Atmospheric Science* 66(9): 2874-2887, [doi:10.1175/2009JAS3029.1](https://doi.org/10.1175/2009JAS3029.1).
- de Boer, G, GJ Tripoli, and EW Eloranta. 2008. "Preliminary comparison of CloudSAT-derived microphysical quantities with ground-based measurements for mixed-phase cloud research in the Arctic." *Journal of Geophysical Research* 113: D00A06, [doi:10.1029/2008JD010029](https://doi.org/10.1029/2008JD010029).
- Eloranta, EW. 2005. "High Spectral Resolution Lidar." In *Lidar: Range-Resolved Optical Remote Sensing of the Atmosphere*, Ed. K Weitkamp, Springer Series in Optical Sciences, Springer-Verlag, New York.
- Klein, SA, R McCoy, H Morrison, A Ackerman, A Avramov, G de Boer, M Chen, J Cole, AD DelGenio, M Falk, M Foster, A Fridlind, J-C Golaz, T Hashino, J Harrington, C Hoose, M Khairoutdinov, V Larson, X Liu, Y Luo, G McFarquhar, S Menon, R Neggers, S Park, K von Salzen, JM Schmidt, I Sednev, B Shipway, M Shupe, D Spangenberg, Y Sud, D Turner, D Veron, G Walker, Z Wang, A Wolf, S Xie, K-M Xu, F Yang, and G Zhang. 2009. "Intercomparison of model simulations of mixed-phase clouds observed during the ARM Mixed-Phase Arctic Cloud Experiment I: Single-layer cloud." *Quarterly Journal of the Royal Meteorological Society* 135(641): 979-1002, [doi:10.1002/qj.416](https://doi.org/10.1002/qj.416).
- Lesins, G, L Bourdages, TJ Duck, JR Drummond, EW Eloranta, and VP Walden. 2009. "Large surface radiative forcing from tropospheric blowing snow residuals measured in the High Arctic at Eureka." *Atmospheric Chemistry and Physics* 9: 1847-1862.
- McMillian, WW, JX Warner, M McCourt Comer, E Maddy, A Chu, L Sparling, E Eloranta, R Hoff, G Sachse, C Barnet, I Razenkov, and W Wolf. 2004. "AIRS views transport from 12-22 July 2004 Alaskan/Canadian fires: Correlation of AIRS CO and MODIS AOD with forward trajectories and comparison of AIRS CO retrievals with DC-8 in situ measurements during INTEX-A/ICARTT." *J. Journal of Geophysical Research* 113, D20301, [doi:10.1029/2007JD009711](https://doi.org/10.1029/2007JD009711).
- O'Neill, NT, O Pancrati, K Baibakov, E Eloranta, RL Batchelor, J Freemantle, LJB McArthur, K Strong, R Lindenmaier. 2008. "Occurrence of weak, sub-micron, tropospheric aerosol events at high Arctic latitudes." *Geophysical Research Letters* 35(14): L14814, [doi:10.1029/2008GL033733](https://doi.org/10.1029/2008GL033733).
- Shupe, MD, JS Daniel, G de Boer, EW Eloranta, P Kollias, E Luke, CN Long, D Turner, and J Verlinde. 2008. "A focus on mixed-phase clouds: The status of ground-based observational methods." *Bulletin of the American Meteorological Society* 89: 1549-1562, [doi:10.1175/2008BAMS2378.1](https://doi.org/10.1175/2008BAMS2378.1).
- Shupe, MD, P Kollias, M Poellot, and E Eloranta. 2008. "On deriving vertical air motions from cloud radar Doppler spectra." *Journal of Atmospheric and Oceanic Technology* 25: 547-557, [doi:10.1175/2007JTECHA1007.1](https://doi.org/10.1175/2007JTECHA1007.1).

Turner, DD, and EW Eloranta. 2008. "Validating mixed-phase cloud optical depth retrieved from infrared observations with high spectral resolution lidar." *IEEE Geoscience and Remote Sensing Letters* 5(2): 285-288, [doi:10.1109/LGRS.2008.915940](https://doi.org/10.1109/LGRS.2008.915940).

